CHAPTER II

NON-RELATIVISTIC POTENTIAL

II.2. Introduction :

The discovery of the heavy quarkonia has led to a very active field of research involving the theoretical predictions of the QCD and some inspired phenomenology guided by the experimental results. Considerable progress has already been made in understanding the properties of these $Q\bar{Q}$ states, considered to be bound by a flavour-independent non-relativistic potential. The observed spin-averaged properties of heavy quarkonia could be explained by different authors with varying degrees of success. However, recent measurement of the fine-hyperfine interactions have led to renewed activities in this field, particularly because the earlier parameters are found to be inadequate. We have considered in this chapter a non-relativistic potential model to study the spectroscopy of heavy quarkonia, particularly those which do not require a relativistic treatment. The study will provide the basic structure for incorporating the relativistic corrections, in particular, the fine-hyperfine interactions, which will be considered in the next chapter. While choosing a potential for the $Q\bar{Q}$ system, we expect the perturbative QCD to be valid at short-distances, while at large distances, a confining potential, possibly a linear one (or a little modification thereof) should be adequate. We have, therefore, considered in this chapter a static potential which consists of a short-range 2-loop QCD potential which is matched to a modified linear potential for

large distances. We have studied in detail the $b\bar{b}$ and $c\bar{c}$ systems. Since the $Q\bar{Q}$ potential is assumed to be flavour independent, the same potential is used to study the toponium states also for a range of possible t-quark masses. The study of toponium is important particularly because the toponium states probe effectively a very short-distance part of the $Q\bar{Q}$ potential which is not probed accurately by the $b\bar{b}$ and $c\bar{c}$ systems. The toponium may provide a possible method of production of the Higgs particle through the decay $T \to H + \gamma$ if allowed kinematically. Lastly, the toponium may provide us with signatures for theories beyond the standard model, in particular, in our search for sparticles.

The scheme of presentation is as follows. In section II.2, we discuss breifly the non-relativistic $Q\bar{Q}$ potential we have taken to calculate the spectroscopy. Calculations of spin-averaged mass spectrum, leptonic decay widths, E1 transition rates of $b\bar{b}$ and $c\bar{c}$ mesons have been done by solving the Schrödinger equation numerically. Various bounds on $t\bar{t}$ quarkonium mass are discussed in section II.3. The predicted energy levels of $t\bar{t}$ systems are also given. By making use of the experimental branching ratio, the total width and hadronic decay width of χ_b^J state are predicted in section II.4. Section II.5 contains some concluding remarks.

II.2. Non-relativistic $Q\bar{Q}$ potential :

The extensive work on the $c\bar{c}$ and $b\bar{b}$ spectroscopy has helped in determining uniquely the $Q\bar{Q}$ static potential within the

range $0.1 \text{ fm} \lesssim r \lesssim 1 \text{ fm}$. In fact, the different potentials[6,61] that fit the spin-averaged data reasonably well all agree within this range. For small distances, the $Q\bar{Q}$ potential should be given accurately by the one-gluon-exchange term with a running coupling constant. This potential upto 2-loop corrections has been considered by a number of authors.[2,62] We, however, make a special choice for the non-relativistic $Q\bar{Q}$ potential

$$V_{Q\bar{Q}}(r) = f(r)V_{QCD}(r) + \left(1 - f(r) \right)V_L(r) \ , \qquad (2.1)$$

where $V_{QCD}(r)$ is the 2-loop QCD potential, V_L is the long-range potential and $f(r)$ is the Woods-Saxon function

$$f(r) = \frac{1 + e^{-r_0/s}}{1 + e^{(r - r_0)/s}} \ . \qquad (2.2)$$

The 2-loop QCD potential, $V_{QCD}(r)$ may be written as[63,76]

$$V_{QCD}(r) = - \frac{4\pi \ C_2(R)}{b_0 \ r \ \ln(1/\Lambda^2_{\overline{MS}} \ r^2)} \left[1 + (2\gamma_E + c/b_0) \frac{1}{\ln(1/\Lambda^2_{\overline{MS}} \ r^2)} \right.$$

$$\left. - \frac{b_1}{b_0^2} \frac{\ln \ln(1/\Lambda^2_{\overline{MS}} \ r^2)}{\ln(1/\Lambda^2_{\overline{MS}} \ r^2)} \right] . \qquad (2.3)$$

In above, γ_E is the Euler constant and

$$b_0 = \frac{11}{3} \ C_2(G) - \frac{2}{3} \ N_f$$

$$b_1 = \frac{34}{3}\left[C_2(G) \right]^2 - \frac{10}{3} C_2(G)\, N_f - 2C_2(R)\, N_f$$

$$c = \frac{31}{9} C_2(G) - \frac{10}{9} N_f \ .$$

In above, $C_2(R)$ and $C_2(G)$ are the invariant quadratic casimir operators, which for $SU(3)_c$ equal 4/3 and 3 respectively. N_f gives the number of quark flavours relevant for the problem, which we choose to be equal to 4. In the standard $\overline{MS}$ scheme, it is customary to choose N_f as the number of quark flavours with mass $\leq \mu$, where μ gives the renormalization scale.

For the long-range potential, we choose the form

$$V_L(r) = Ar + B \left(\ln \Lambda_{\overline{MS}}\, r + 1 \right) \ . \qquad (2.4)$$

We have included the logarithmic term to take into account a small modification of the linear potential. The reason for the choice will be explained in the next chapter. The Woods-Saxon function interpolates smoothly between the short-range potential and the long-range part. The position and the extension of the cross-over region can be fixed by varying the parameters r_0 and s. However, the variation of s is limited within a narrow range, since the cross-over region is approximately known. Combinations of different potentials have been studied by several authors.[64,65] We have followed, in particular, Igi and Hikasa.[63]

We have solved numerically the Schrödinger equation with potential (2.1). We have developed a comprehensive computer

programme for the relevant calculations. We have chosen $\Lambda_{\overline{MS}}$ = 0.196 GeV, M_b = 4.783 GeV and M_c = 1.364 GeV respectively. Bound state masses of $Q\bar{Q}$ systems are obtained from Eq.(1.1) of the first chapter. The parameters of the potential giving the best fit are r_0 = 0.105 fm , s = 0.02 fm, A= 0.019 GeV^2, B = 0.677 GeV. Since no spin-dependent interactions are considered in this chapter, a direct comparison with experimental results is not always possible. Thus the calculated spin-averaged 1S state of $b\bar{b}$ has a mass of 9445.5 MeV while experimental value for $^3S_1$ state is 9460.32 ± 0.22 MeV. The other state $^1S_0$ has not yet been discovered. The problem will be taken up in the next chapter. The agreement with the experimental result is reasonably good. In Ref.(66), the authors have matched the 1S levels with the experimental value without performing fine-hyperfine calculations. It is, however, expected that the inclusion of the fine-hyperfine contribution will shift the energy levels upwards. In that case, the input quark masses will have to be adjusted for better agreement. For the $c\bar{c}$ system, we vary the input c-quark mass so as to obtain the spin-averaged masses. This gives $M_{1S}(c\bar{c})$ = 3068.7 MeV and $M_{2S}(c\bar{c})$ = 3662.8 MeV respectively. The experimental results for these states, determined very accurately, are $M_{1S}(c\bar{c})$ = 3067.93 ± 1.16 MeV and $M_{2S}(c\bar{c})$ = 3663 ± 1.15 MeV, giving an excellent agreement. In Table 2.1, the spin-averaged masses for $b\bar{b}$ and $c\bar{c}$ systems are shown. However, in the case of 1P and 2P states of $b\bar{b}$, we can compare only the centre of gravity mass values. The value of 1P state is shifted downwards by about 15 MeV

Table 2.1. Calculated energy values of the $b\bar{b}$ and $c\bar{c}$ states.

Bound state	Spin-averaged mass of $b\bar{b}$ system(MeV)	Spin-averaged mass of $c\bar{c}$ system(MeV)
1S	9445.5	3068.7
2S	10030.0	3662.8
3S	10358.0	4009.6
4S	10593.0	4265.6
1P	9885.8	3505.2
2P	10257.0	3897.1
1D	10155.0	3784.0
2D	10433.0	4083.0

for both the flavours. The reason for this shift will be discussed later on. In Figs. 2.1, 2.2 and 2.3, we show the variation of the energy difference as a function of $\Lambda_{\overline{MS}}$, r_o and s. We represent the differences as Δ_1 and Δ_2 where Δ_1 = E(1P) - E(1S) and Δ_2= E(2P)- E(1S) respectively.

We have also calculated the leptonic decay widths and E1 transition rates of heavy quarkonia. In calculating the leptonic width we included the Poggio-Schnitzer (PS) correction to the Van-Royen-Weisskopf formula, given in the first chapter. The leptonic widths along with the PS correction are presented in the Table 2.2. It is seen that the value of PS correction factor for the $c\bar{c}$ and $b\bar{b}$ systems is about 0.4 to 0.8. As can be seen from Table 2.2, the results for $c\bar{c}$ system with PS correction are in better agreement with the experimental values. However, in the case of $b\bar{b}$ states, it is clear that the PS correction is not necessary. This is expected, as for $b\bar{b}$ systems, the relevant distance scales are such that the 2-loop QCD potential, which already incorporates the vacuum polarization effect is dominant and no further correction is required.

The E1 transition rates of heavy quarkonia between an initial state i and a final state f are given by the Eqs. (1.3) and (1.4). The photon energy ω may be expressed as

$$\omega = \frac{M^2(v_1) - M^2(v_2)}{2M(v_1)} \quad , \quad M(v_1) > M(v_2) \; . \qquad (2.5)$$

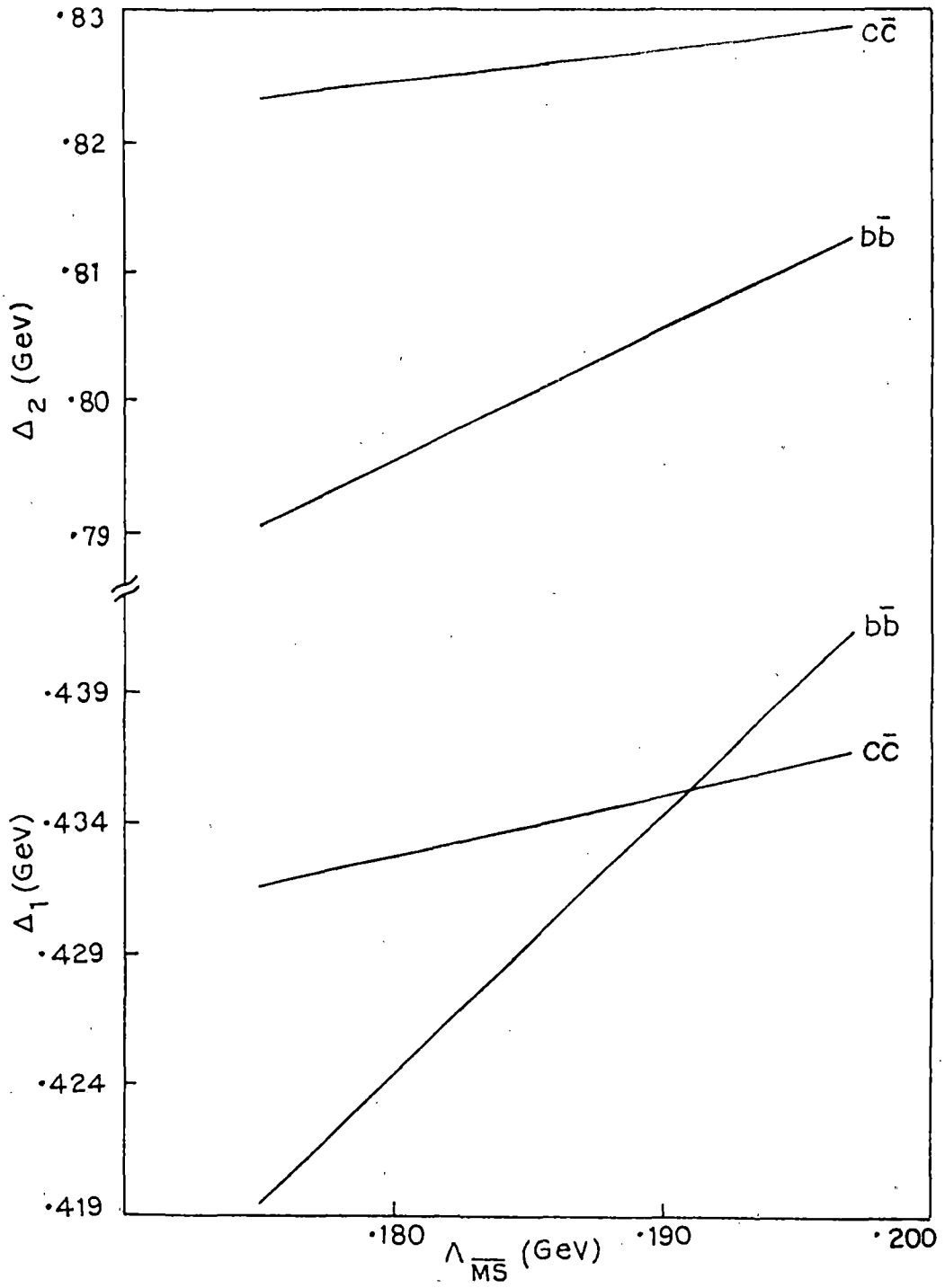

Fig.2.1. Variation of $\Delta_1 = E(1P) - E(1S)$ and $\Delta_2 = E(2P) - E(1S)$ with $\Lambda_{\overline{MS}}$.

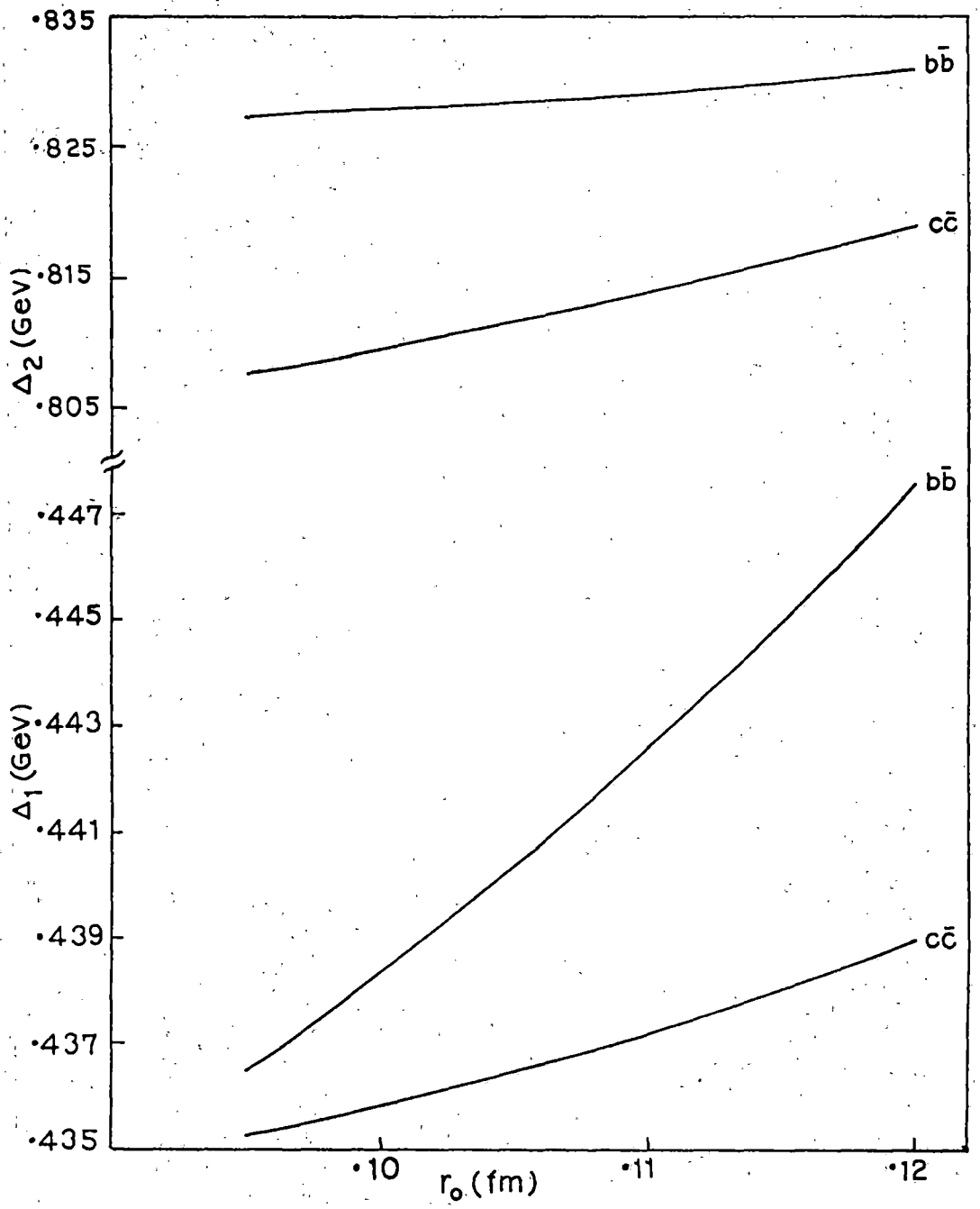

Fig.2.2. Variation of $\Delta_1 = E(1P) - E(1S)$ and $\Delta_2 = E(2P) - E(1S)$ with r_o .

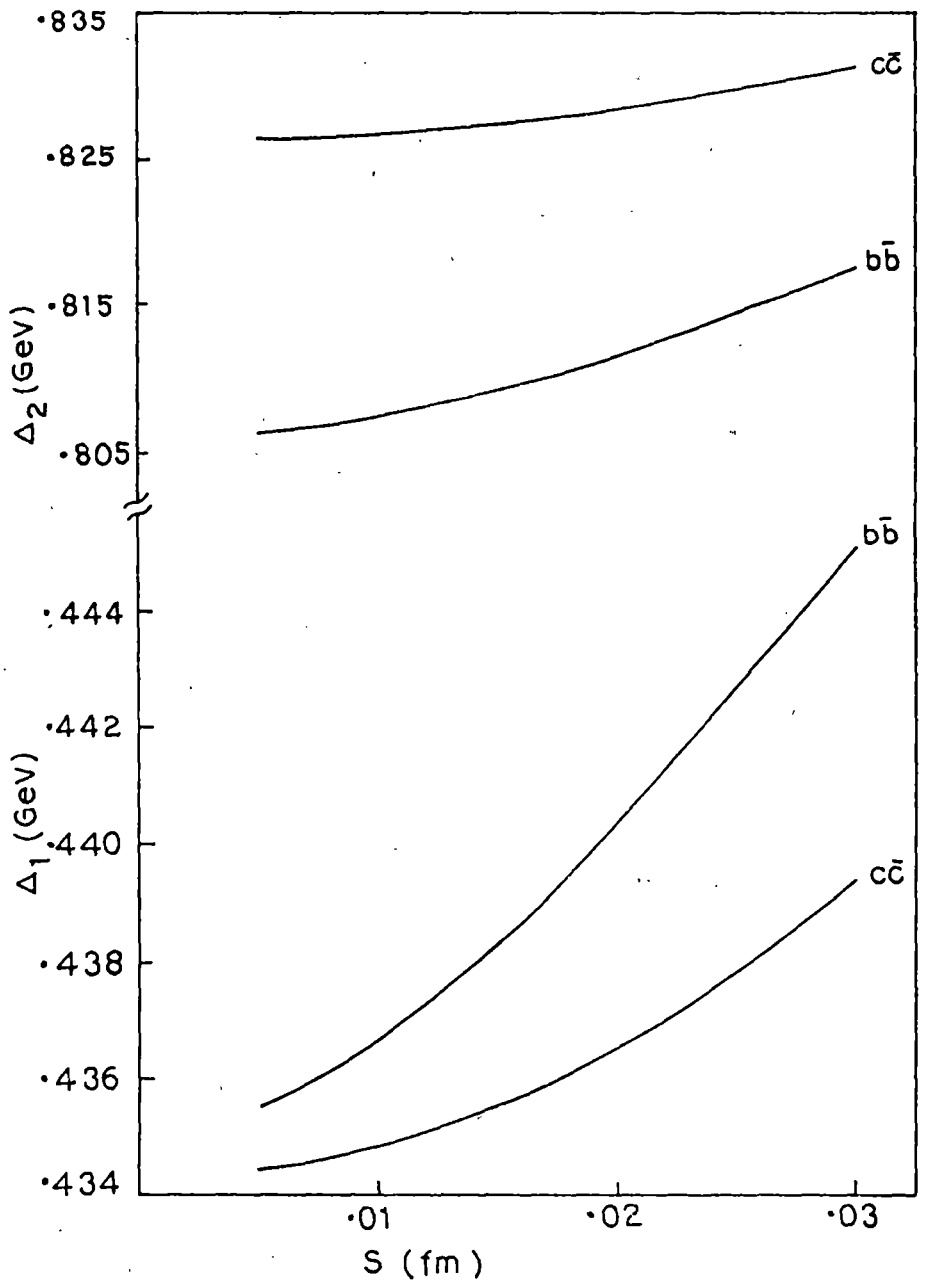

Fig.2.3. Variation of $\Delta_1 = E(1P) - E(1S)$ and $\Delta_2 = E(2P) - E(1S)$ with s .

Table 2.2. Predicted leptonic decay widths of $b\bar{b}$ and $c\bar{c}$ systems without and with Poggio-Schnitzer corrections. Experimental values are taken from Ref.(28).

State	$\lvert \phi(0) \rvert^2$ (GeV^3)	Experimental (KeV)	Uncorrected (KeV)	Poggio-Schnitzer corrected (KeV)
Y(9.460)	5.1738	1.34 ± 0.05	1.373	1.087
Y(10.023)	2.5943	0.60 ± 0.036	0.611	0.462
Y(10.355)	1.8058	0.44 ± 0.03	0.398	0.294
Y(10.580)	1.4192	0.24 ± 0.05	0.299	0.217
ψ(3.097)	0.7088	4.72 ± 0.35	7.127	4.559
ψ(3.685)	0.3832	2.14 ± 0.21	2.704	1.468
ψ(4.040)	0.2766	0.75 ± 0.15	1.629	0.801
ψ(4.415)	0.2327	0.47 ± 0.10	1.211	0.553

Since we have not considered the fine-hyperfine structure in this chapter, we calculate this rates using available experimental values of ω. We have given our results in Table 2.3 and 2.4. We compare our results with the results of some other workers.[51,67,45] Kwong *et al.*[67] used the inverse scattering method to construct the $Q\bar{Q}$ potential. Our results almost agree with the results of the models of Ref. (51) and (67). We have also shown in Table 2.5 the values of the electric dipole matrix elements which are evaluated non-relativistically. The transition rates of $3S \rightarrow 1P$ for $b\bar{b}$ system are very small due to cancellations in the overlap integral for the 3S and 1P wave-functions. This point was also mentioned by Fulcher.[68] In case of $c\bar{c}$, we obtain higher values than the observed rates. This is because the relativistic effects are more important for $c\bar{c}$ than for $b\bar{b}$ system and the relativistic correction is very important for these transition rates.

II.3. t-quark mass and Toponium :

Recent experimental results indicate that the mass of the top quark does not lie around 50 GeV as suggested earlier by the UA1 experimental group at CERN.[29] However, some suitable signatures for detection of the t-quark have been identified[69] recently. One now expects direct as well as indirect signals for the presence of t-quark in the next generation collider energy range, if not earlier. The indirect evidence for a t-quark comes

Table 2.3. E1 transition rates for $b\bar{b}$ system. Experimental values of ω are taken from Ref.(28).

Transition	Experimental ω (MeV)	Transition width (KeV)				Experimental width (KeV)
		MR[45]	FUL[51]	KR[67]	OURS	
$2^3S_1 \rightarrow 1^3P_0$	162.3 ± 1.3	1.0	1.38	1.39	1.277	1.29 ± 0.31
1^3P_1	130.6 ± 0.7	2.1	2.17	2.18	2.000	2.01 ± 0.49
1^3P_2	109.6 ± 0.6	2.2	2.13	2.14	1.966	1.98 ± 0.48
$3^3S_1 \rightarrow 1^3P_0$	483.8 ± 1.4	0.025	0.005	0.007	0.010	
1^3P_1	453.2 ± 0.9	0.025	0.011	0.017	0.026	0.04 ± 0.03
1^3P_2	432.8 ± 0.8	0.15	0.016	0.025	0.037	0.06 ± 0.05
$3^3S_1 \rightarrow 2^3P_0$	119.3 ± 1.1	1.4	1.35	1.65	1.475	1.22 ± 0.3
2^3P_1	99.6 ± 0.4	2.8	2.36	2.52	2.575	3.08 ± 0.6
2^3P_2	85.9 ± 0.7	2.7	2.53	2.78	2.753	3.26 ± 0.7
$1^3P_0 \rightarrow 1^3S_1$	391.7 ± 1.3	31	30.8	26.1	27.917	
1^3P_1	422.5 ± 0.7	36	38.6	32.8	35.034	
1^3P_2	442.9 ± 0.6	38	44.5	37.8	40.357	
$2^3P_0 \rightarrow 1^3S_1$	741.5 ± 2.3	7.5	7.62	8.48	6.744	
2^3P_1	764.8 ± 0.8	12	8.19	9.31	7.400	
2^3P_2	776.8 ± 0.7	14	8.60	9.75	7.753	
$2^3P_0 \rightarrow 2^3S_1$	205.0 ± 2.3	12	13.0	11.3	12.390	
2^3P_1	229.7 ± 0.9	14	17.0	15.9	17.430	
2^3P_2	242.3 ± 0.8	16	20.1	18.7	20.459	

Table 2.4. E1 transition rates for $c\bar{c}$ system. Experimental values of ω are used.

Transition	Experimental ω (MeV)	Transition width (KeV)	
		MR[45]	OURS
$1^3P_0 \rightarrow 1^3S_1$	303.2	226	186.33
1^3P_1	388.7	460	392.60
1^3P_2	429.4	609	529.28
$2^3S_1 \rightarrow 1^3P_0$	261.0	37	69.83
1^3P_1	171.8	48	59.75
1^3P_2	127.7	41	40.90

Table 2.5. Dipole matrix element $\langle r \rangle = \int R\, R' r^3\, dr$ for $b\bar{b}$ and $c\bar{c}$ systems.

Transition	$\langle r \rangle$ (GeV^{-1}) $(b\bar{b})$				$\langle r \rangle$ (GeV^{-1}) $(c\bar{c})$	
	FUL[51]	KR[67]	MR[45]	OURS	MR[45]	OURS
$1^3P_J \rightarrow 1^3S_1$	1.194	1.098	1.08	1.135	2.08	2.15
$2^3S_1 \rightarrow 1^3P_J$	-1.644	-1.646	1.64	-1.577	2.65	-2.86
$2^3P_J \rightarrow 1^3S_1$	0.226	0.240	0.26	0.214		0.37
$2^3P_J \rightarrow 2^3S_1$	1.970	1.911	1.89	1.998		3.72
$3^3S_1 \rightarrow 1^3P_J$	0.0185	0.023	-0.024	-0.028		-0.07
$3^3S_1 \rightarrow 2^3P_J$	-2.573	-2.672	2.68	-2.689		-4.83

from the observed forward-backward asymmetry in $e^+e^- \rightarrow \bar{b}b$ as well as the absence of flavour changing neutral decay of b quark. The indirect constraints $40 < M_t < 200$ GeV on the top quark mass are available from i) the radiative correction to W and Z boson masses and ii) the $B_d - \bar{B}_d$ mixing. A direct quark search, on the otherhand, may be available in the e^+e^- collider although the current energy range is rather low. The data from PETRA and TRISTAN[70] suggest $M_t > 26$ GeV. The next generation LEPI and LEPII colliders are expected to probe t-quark mass upto 50 GeV and 100 GeV respectively. The $p\bar{p}$ colliders seem to be more promising in this respect because of their high energy reach. However, the corresponding t-signal is not very clean and one has to use isolated electron (muon) signature.[71] The current data from the CERN $p\bar{p}$ collider[72] suggest $M_t > 40$ GeV, conforming with the theoretical lower limit. In near future $p\bar{p}$ data from the Tevatron and the upgraded CERN colliders are expected to probe the upper mass limit[73] of the t-quark mass. These results are expected to be available by mid-nineties. The CDF collaboration at the Tevatron and UA1 and UA2 at CERN have put the experimental limit on top quark mass above or at least 60 GeV.[74] We shall confine our discussions here to the range $30 \leq M_t \leq 70$ GeV.

Table 2.6 gives some predicted toponium levels for different values of top quark mass. For $M(t\bar{t}) \sim 80$ GeV, we expect about 10 S-states below the threshold. A graph of the variation of the binding energies versus the mass of t-quark is shown in Fig.2.4 and its nature is found to be almost linear. The levels

Table 2.6. Energy levels of $t\bar{t}$ states.

Mass of t quark (GeV)	Energy levels for various states in GeV			
	1S	2S	1P	2P
30	59.15	59.78	59.64	60.02
35	69.07	69.71	69.58	69.97
40	79.01	79.66	79.53	79.92
45	88.95	89.60	89.49	89.87
50	98.89	99.56	99.45	99.84
55	108.84	109.51	109.41	109.80
60	118.78	119.48	119.38	119.77
65	128.73	129.44	129.35	129.74
70	138.68	139.40	139.32	139.71

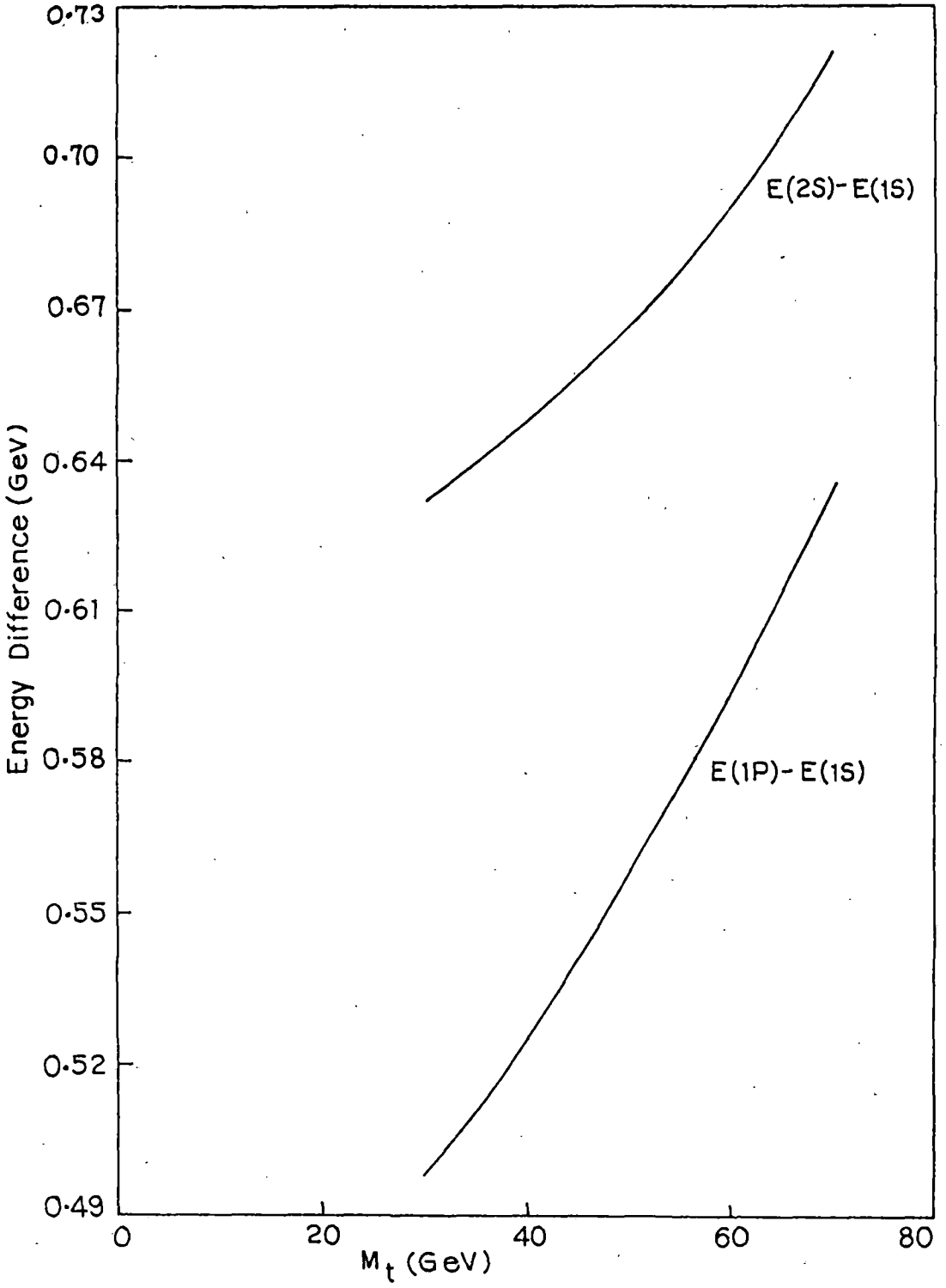

Fig. 2.4. Level Separation VS. top quark mass.

are not yet coulombic.

II.4. Total and hadronic decay widths of χ_b^J states :

The Crystal Ball Collaboration at DESY[19] have studied radiative decays of the Y(2S) resonance in which they detected two monochromatic photon lines at energies (107.0 ± 1.1 ± 1.3) MeV and (131.7 ± 0.9 ± 1.3) MeV along with a pair of leptons. The decay mechanism may be written as

$$\begin{aligned} Y(2S) &\rightarrow \gamma + \chi_b \\ &\qquad \hookrightarrow \gamma + Y(1S) \\ &\qquad\qquad \hookrightarrow e^+e^- \text{ or } \mu^+\mu^- \ . \end{aligned} \tag{2.6}$$

The product branching ratio is given by

$$\begin{aligned} BR_J\ [\ Y(2S) \rightarrow \gamma\gamma l^+l^-\ ] \equiv BR\ [\ Y(2S) \rightarrow \gamma\chi_b^J\ ] \times BR\ [\ \chi_b^J \rightarrow \gamma Y(1S)\ ] \\ \times BR\ [\ Y(1S) \rightarrow l^+l^-\ ] \end{aligned} \tag{2.7}$$

By making use of the experimental branching ratio, we can find out the total width and hadronic decay width of χ_b^J state, which is given by

$$\Gamma_{had}(\chi_b^J) = \Gamma_\gamma(\chi_b^J) \times \left[\frac{1}{BR\left(\chi_b^J \rightarrow \gamma\ Y(S)\right)} - 1 \right] . \tag{2.8}$$

Our calculated results are as follows :

(1) Calculated E1 transition widths :

Transition	Transition width in KeV
$1^3P_1 \rightarrow 1^3S_1$	35.034
$1^3P_2 \rightarrow 1^3S_1$	40.357
$2^3S_1 \rightarrow 1^3P_1$	2.000
$2^3S_1 \rightarrow 1^3P_2$	1.966

(2) We make use of the experimental values of the branching ratios[18]

$$BR_2 [\ \Upsilon(2S) \rightarrow \gamma\chi_b^2\ ] = (\ 5.8 \pm 0.7 \pm 1.0\ )\%$$

$$BR_1 [\ \Upsilon(2S) \rightarrow \gamma\chi_b^1\ ] = (\ 6.5 \pm 0.7 \pm 1.2\ )\%$$

to determine roughly the average total width of $\Upsilon(2S)$ ~ 33 KeV, which may be compared with the experimental results (44 ± 9) KeV.

(3) We next consider the χ_b^J states : From (2) above and the measured values of the product branching ratio $BR_2[\Upsilon(2S) \rightarrow \gamma\gamma l^+l^-] = (\ 4.4 \pm 0.9 \pm 0.5\ ) \times 10^{-4}$ and $BR_1[\Upsilon(2S) \rightarrow \gamma\gamma l^+l^-] = (\ 5.8 \pm 0.9 \pm 0.7\ ) \times 10^{-4}$, given by Crystal Ball Collaboration[19] and average branching ratio for $\Upsilon(1S) \rightarrow l^+l^-$ ~ 0.027,[28] we get the total width and the hadronic width of χ_b^J:

	Total width (KeV)	Hadronic width (KeV)
χ_b^2	143.63	103.27
χ_b^1	106.01	70.98

Since there is no measured value of the product branching ratio for χ_b^0 , we cannot determine its width, even if we have the E1

transition rates involving the χ_b^0 state. The experimental results involving χ_b^0 will be very much welcome.

II.5. Conclusions :

We have shown that the non-relativistic description of the heavy quarkonia by a potential comprising of a short-range QCD potential which is matched to a confining potential generates the mass spectrum and decay widths of the $b\bar{b}$ as well as $c\bar{c}$ states. We find that the values of the leptonic widths including Poggio-Schnitzer corrections are in good agreement with experiments in the case of $c\bar{c}$ states. However, this correction is negligible for heavy quarkonia. We are unable to find a good fit of E1 transition rates of $c\bar{c}$ due to the fact that we neglected the relativistic as well as coupled channel effects, which reduce the overlap between the two states considerably. It is expected that the parameters of the potential may require slight adjustment while calculating relativistic effects. Since the branching ratio of $b\bar{b}$ state has not been determined theoretically by us here, we use experimental branching ratio to determine the total width and hadronic width of the χ_b^1 and χ_b^2 states. The results show the overall efficacy of a non-relativistic description for the Heavy quarkonia. However, for quantitative agreement with experimental results, one should include spin-dependent interactions, which are relativistic in nature. This will be taken up in the next chapter.